

Amyloid β -Protein Fibrillogenesis

DETECTION OF A PROTOFIBRILLAR INTERMEDIATE*

(Received for publication, April 21, 1997, and in revised form, June 18, 1997)

Dominic M. Walsh[‡], Aleksey Lomakin^{‡§}, George B. Benedek[§], Margaret M. Condrón[‡],
and David B. Teplow^{‡¶}

From the [‡]Department of Neurology (Neuroscience), Harvard Medical School, and Biopolymer Laboratory, Brigham & Women's Hospital, Boston, Massachusetts 02115 and the [§]Department of Physics and Center for Materials Science and Engineering, Massachusetts Institute of Technology, Cambridge, Massachusetts 02139

Fibrillogenesis of the amyloid β -protein ($A\beta$) is a seminal pathogenetic event in Alzheimer's disease. Inhibiting fibrillogenesis is thus one approach toward disease therapy. Rational design of fibrillogenesis inhibitors requires elucidation of the stages and kinetics of $A\beta$ fibrillogenesis. We report results of studies designed to examine the initial stages of $A\beta$ oligomerization. Size exclusion chromatography, quasielastic light scattering spectroscopy, and electron microscopy were used to characterize fibrillogenesis intermediates. After dissolution in 0.1 M Tris-HCl, pH 7.4, and removal of pre-existent seeds, $A\beta$ chromatographed almost exclusively as a single peak. The molecules composing the peak had average hydrodynamic radii of 1.8 ± 0.2 nm, consistent with the predicted size of dimeric $A\beta$. Over time, an additional peak, with a molecular weight $>100,000$, appeared. This peak contained predominantly curved fibrils, 6–8 nm in diameter and <200 nm in length, which we have termed "protofibrils." The kinetics of protofibril formation and disappearance are consistent with protofibrils being intermediates in the evolution of amyloid fibers. Protofibrils appeared during the polymerization of $A\beta$ (1–40), $A\beta$ (1–42), and $A\beta$ (1–40)-Gln²², peptides associated with both sporadic and inherited forms of Alzheimer's disease, suggesting that protofibril formation may be a general phenomenon in $A\beta$ fibrillogenesis. If so, protofibrils could be attractive targets for fibrillogenesis inhibitors.

Fibrillar amyloid plaques in the cerebral parenchyma and vasculature are a cardinal neuropathologic feature of Alzheimer's disease (AD)¹ (1). Plaques are composed predominantly of insoluble fibers of the amyloid β -protein ($A\beta$) (2). $A\beta$ is a normal component of the plasma and cerebrospinal fluid, occurring as a soluble 40- or 42-residue peptide (3, 4). Thus, a central question in the etiology of AD is the mechanism(s) by

which these soluble $A\beta$ molecules are converted into plaque-associated fibers (5). This question is particularly relevant because $A\beta$ fibers, unlike nonfibrillar $A\beta$, are neurotoxic *in vitro* and are associated with damaged neuropil *in vivo* (6). These observations suggest that inhibiting fiber formation would be an effective approach toward AD therapy. However, if these efforts are to succeed, fiber formation must be understood at the molecular level.

$A\beta$ fibrillogenesis is a nucleation-dependent polymerization process (7, 8). The kinetics of this type of process is controlled by two key parameters, nucleation rate and elongation rate. Past studies of the kinetics of $A\beta$ fibrillogenesis, utilizing techniques including turbidity, sedimentation, and thioflavine T binding, could only provide information on the appearance of high molecular weight aggregates (7, 9) or the disappearance of soluble peptide (10–13). Neither rate constants nor structures of fibrillogenesis intermediates could be determined by these approaches. In contrast, the technique of quasielastic light scattering spectroscopy (QLS) is particularly well suited for resolving individual stages of polymerization processes and for examining polymerization kinetics (14). QLS was used initially to monitor late stages of $A\beta$ fibrillogenesis (15, 16). Recently, however, a model system was developed for the highly reproducible growth of $A\beta$ fibers (8). This allowed QLS monitoring of polymer size during all phases of fibrillogenesis and determination of the rates of $A\beta$ fibril nucleation and elongation (8).

The QLS approach is less useful for studying small structures, such as $A\beta$ monomers and oligomers, when they exist in mixtures with larger polymers. Because these prefibrillar intermediates are potential targets for fibrillogenesis inhibitors, it is important to characterize them. One method for doing so is SDS-PAGE (17–20). However, since many $A\beta$ polymers are SDS-labile, interpreting SDS-PAGE studies of $A\beta$ polymerization is problematic. Size exclusion chromatography (SEC) is an attractive alternative to SDS-PAGE because it fractionates on the basis of molecular weight and is performed using nondenaturing and nondisaggregating buffers. SEC has been used to study the aggregation state of $A\beta$ in solution (20–23), but its potential in kinetic studies has not been exploited. We report here the use of SEC, coupled with QLS and electron microscopy, to characterize the temporal evolution and structures of oligomeric intermediates in the pathway of $A\beta$ fibrillogenesis.

EXPERIMENTAL PROCEDURES

Chemicals and Solvents

Chemicals were obtained from Sigma and, unless otherwise stated, were of the highest purity available. Solvents were HPLC grade and were obtained from Fisher. Water was double-distilled and deionized using a Milli-Q system (Millipore Corp., Bedford, MA).

* This work was supported in part by National Institutes of Health Grants 1P01AG14366 (to D. B. T.) and 5R37EY05127 (to G. B. B.) and by the Foundation for Neurologic Diseases (to D. B. T.). The costs of publication of this article were defrayed in part by the payment of page charges. This article must therefore be hereby marked "advertisement" in accordance with 18 U.S.C. Section 1734 solely to indicate this fact.

¶ To whom correspondence should be addressed: Brigham & Women's Hospital, 77 Avenue Louis Pasteur (HIM-756), Boston, MA 02115. Tel.: 617-525-5270; Fax: 617-525-5252; E-mail: teplow@cnd.bwh.harvard.edu.

¹ The abbreviations used are: AD, Alzheimer's disease; $A\beta$, amyloid β -protein; QLS, quasielastic light scattering spectroscopy; PAGE, polyacrylamide gel electrophoresis; SEC, size exclusion chromatography; HPLC, high pressure liquid chromatography; HFIP, 1,1,1,3,3,3-hexafluoro-2-propanol; RIA, radioimmunoassay; Tricine, N-[2-hydroxy-1,1-bis(hydroxymethyl)ethyl]glycine.

Peptides

Peptides were synthesized as described by Lomakin *et al.* (8). Crude A β -(1–40) was purified by reverse phase HPLC using a Vydac phenyl column (22 \times 250 mm) and a linear gradient of 28–56% B over 50 min (A: 0.1% (v/v) trifluoroacetic acid; B: 70% (v/v) acetonitrile (CH₃CN), 0.09% (v/v) trifluoroacetic acid) at a flow rate of 20 ml/min. A β -(1–42) was purified using a PLRP-S column (25 \times 150 mm) and a linear gradient of 20–60% B over 80 min (A: 50 mM Tris-HCl, pH 9.1; B: 50 mM Tris-HCl, pH 9.1, containing 54% (v/v) CH₃CN and 6% (v/v) 2-propanol) at a flow rate of 15 ml/min (24). Following purification, A β -(1–42) was dialyzed against 0.15 M ammonium hydroxide in 40% (v/v) CH₃CN, lyophilized, and converted to its trifluoroacetic acid salt by dissolution in 100% trifluoroacetic acid. Peptide mass, purity, and quantity were determined by a combination of matrix-assisted laser desorption/ionization time-of-flight mass spectrometry, analytical HPLC, and quantitative amino acid analysis, respectively. Purified peptides were aliquoted, lyophilized, and stored at -20°C until used. A β -(40–1) was generously provided by Dr. Dennis Selkoe (Brigham & Women's Hospital and Harvard Medical School).

SEC

Columns and Buffers—A description of columns and buffers is found in Table I. Superdex, Superose and TSK columns were attached to a Rainin HPLC system consisting of a HPXL pump, a Rheodyne 7161 injector, and a Dynamax UV-1 detector. Columns were eluted at a flow rate of 0.5 ml/min and peptides detected by UV absorbance at 254 nm. Sephadex G-50 (superfine) media were prepared using either 1 \times 30 cm or 1 \times 50 cm borosilicate Econo-columns (Bio-Rad, Hercules, CA) and eluted at 0.17 ml/min using an LKB Microperplex S peristaltic pump. Peptides were detected by UV absorbance at 254 nm using a Pharmacia UV-1 single path monitor. Each experiment was performed at least two times. Pre-packed columns were washed with 50% (v/v) formic acid between experiments. Sephadex columns were prepared from fresh resin prior to each experiment.

Sample Preparation—400 μg of A β -(1–40) were dissolved in 200 μl of water and then vortexed briefly. 200 μl of 2 \times buffer were then added, and the sample was vortexed again. Following centrifugation (17,000 \times g, 3 min), 100 μl of the supernatant was chromatographed. For kinetic analyses, samples were incubated at room temperature for various periods prior to centrifugation. For quasielastic light scattering spectroscopy, electron microscopy, and gel electrophoresis, A β -(1–40) was dissolved at a concentration of 2 mg/ml (0.46 mM), incubated at room temperature for 48 h, and then chromatographed as above. Similarly, A β -(1–40)-Gln²² and A β -(1–42) were dissolved at concentrations of 1 mg/ml (0.23 and 0.22 mM, respectively) and incubated at room temperature for 6 h, and then 300 μl of each were chromatographed as above. Peak fractions of 50–200- μl volume were collected and analyzed.

Preparation of "Seedless" Samples—Disaggregation experiments were performed by dissolving 800 μg of A β -(1–40) in 160 μl of 1,1,1,3,3,3-hexafluoro-2-propanol (HFIP) and incubating at room temperature for 10 min. The HFIP was removed by evaporation under a gentle stream of argon, leaving a slightly yellow film that was resuspended in 80 μl of dimethyl sulfoxide (Me₂SO) and sonicated for 30 min. The solution was then filtered through an Anotop 10 Plus filter (20 nm, Whatman Inc., Clifton, NJ) and diluted 1:9 (v/v) with 0.1 M Tris-HCl, pH 7.4, containing 0.02% (w/v) sodium azide (Tris buffer). After centrifugation (17,000 \times g, 3 min), 100 μl of supernatant were injected onto a Superdex 75 column. The remainder of the solution was incubated at room temperature and sampled at 1, 4, 8, and 24 h.

Radiotracer Experiments—To search for low abundance intermediates, radioiodinated A β -(1–40) (¹²⁵I-A β , ~2000 Ci/mmol) was prepared according to Maggio *et al.* (25) at a final concentration of 100 pM in Tris buffer containing 0.5% (v/v) Me₂SO. After incubation at room temperature for 0, 8, or 24 h, samples were centrifuged (17,000 \times g, 3 min), and 100- μl aliquots were injected onto a Superdex 75 column. 0.5-ml fractions were collected, and their radioactivity was determined by scintillation counting. To examine the effect of varying A β concentration, 3 μl of appropriately diluted A β -(1–40) were added to 597 μl of Tris buffer containing 100 pM ¹²⁵I-A β , to yield final A β concentrations of 1 \times 10⁻¹⁰, 1 \times 10⁻⁹, 1 \times 10⁻⁷, 1 \times 10⁻⁵, and 2.3 \times 10⁻⁴ M. Samples were then incubated and analyzed as above.

Radioimmunoassay (RIA) of Column Fractions—A RIA procedure was used to detect trace levels of oligomeric fibril intermediates. A β -(1–40) was dissolved in HFIP, lyophilized, dissolved to a suitable concentration in Me₂SO, and then diluted 1:200 (v/v) with 0.1 M Tris buffer. Final A β concentrations were 1 \times 10⁻⁷, 1 \times 10⁻⁶, 1 \times 10⁻⁵, and 1 \times 10⁻⁴ M. Samples were then incubated and chromatographed as in the

radiotracer experiments. Fractions were frozen at -20°C until assayed. A β -(1–40) content in each fraction was determined by RIA (26).

QLS

Fractions from SEC were collected directly into cuvettes and analyzed within 1 min of elution. QLS was carried out essentially as described (8). Measurements were performed at 25 $^{\circ}\text{C}$ using a Langley Ford model 1097 autocorrelator and Coherent argon ion lasers (model Innova 90 or Innova 90-plus) operated at 514 nm.

Electron Microscopy

10 μl of sample were applied to carbon-coated Formvar grids (Electron Microscopy Sciences, Washington, PA) and incubated for 60 s. The droplet was then displaced with an equal volume of 0.5% (v/v) glutaraldehyde solution and incubated for an additional 60 s. The grid then was washed with four or five drops of water and wicked dry. Finally, the peptide was stained with 10 μl of 2% (w/v) uranyl acetate solution (Ted Pella, Inc., Redding, CA) for 2 min. This solution was wicked off, and the grid was air-dried. Samples were examined using a JEOL CX100 electron microscope. To examine insoluble material, pellets of A β were suspended in a small volume of buffer and prepared as above.

Gel Electrophoresis

SDS-PAGE was carried out on 16.5% Tricine gels as described by Schagger and Von Jagow (27). Aliquots of each chromatographic fraction (20 μl) were mixed with 3 \times SDS sample buffer (10 μl) and boiled for 5 min immediately prior to electrophoresis. Gels were silver-stained using the Bio-Rad silver stain kit and photographed.

RESULTS

Oligomerization of A β -(1–40)—To monitor oligomerization of A β , an analytical method is necessary that can resolve monomeric A β and its oligomers under nondenaturing, nondisaggregating conditions. We reasoned that SEC would be appropriate for this purpose. Initial analysis of presumably monomeric A β revealed a single peak with a molecular weight of 10,000 (Table I). This unexpectedly high molecular weight suggested that A β might not be monomeric or was partially excluded from the column matrix, indicating a nonideal analyte-matrix interaction.

Because accurate molecular weight determination was critical for the proper interpretation of our experiments, we determined whether the chromatographic behavior of A β varied depending on column matrix or elution conditions (Table I). When A β -(1–40) from the same peptide lot was dissolved in phosphate-buffered saline and chromatographed on Superdex 75 (dextran-agarose), Superose 12 (agarose), or TSK (silica) matrices, the relative molecular weight of A β varied from 10,000 to 18,000. Similarly, when A β -(1–40) was dissolved in 0.1 M Tris-HCl, pH 7.4, and then analyzed, molecular weights of 9,000–15,000 were observed. Other solvent conditions resulted in M_r values ranging from 5,000 to 10,500. One explanation for the variations in M_r was nonideal chromatographic behavior of A β . This was confirmed in experiments in which the elution buffer was modified by the addition of ethylene glycol, an agent used to inhibit solute-column interactions. Under these conditions, a concentration-dependent decrease in A β M_r from 10,000 to 6,000 was seen. We also found that M_r values varied depending on the calibration standards used. Thus, for consistency, all columns were calibrated using the same five standards.

In each experiment, A β -(1–40) chromatographed as a single peak in the included volume of the column, but because of its nonideal behavior, the oligomerization state of A β within these peaks was unclear. If noncovalent multimers composed these peaks, then treating A β with strong denaturants or solvents prior to chromatography might disaggregate these complexes and reduce the M_r . In fact, pretreatment of A β with SDS-PAGE sample buffer, Me₂SO, HFIP, or 90% formic acid, had no effect on its M_r . In addition, A β -(40–1), the "reverse" peptide of A β -(1–40) and one that does not polymerize readily, co-eluted with

TABLE I
Chromatographic properties of $A\beta$ (1-40)

$A\beta$ (1-40) was chromatographed on five different size exclusion media, as described under "Experimental Procedures." For each study, the appropriate column was equilibrated with at least three column volumes of elution buffer and then calibrated with five molecular weight standards: avian ovalbumin (44,000); equine myoglobin (17,000); equine cytochrome C (12,384); bovine aprotinin (6,500); and vitamin B₁₂ (1,350). Standard curves were constructed by regression analysis and used to determine the molecular weights of analytes. Each condition yielded one peak, which decreased in size over 24 h. A small void peak appeared after 24 h of incubation in some experiments.

Column	Separation range (kDa)	Elution buffer ^a	$A\beta$ M_r	Void peak	Correlation coefficient (r^2)
Superdex 75 (1 × 30 cm)	3-70	PBS	10,000	-	0.98
		PBS, 20% sucrose	10,500	-	0.98
		PBS, 20% MPD	9,000	-	0.96
		PBS, 20% ethylene glycol	8,000	±	0.98
		PBS, 50% ethylene glycol	6,000	±	0.98
		0.1 M Tris-HCl, pH 7.4	15,000	+	0.81
Superdex 200 (1 × 30 cm)	10-600	0.1 M Tris-HCl, pH 7.4	14,000	+	0.77
Superose 12 (1 × 30 cm)	1-300	0.1 M Tris-HCl, pH 7.4	15,000	+	0.79
		PBS	12,000	±	0.92
TSK G2000sw (0.7 × 30 cm)	5-100	0.1% trifluoroacetic acid	8,000	-	0.85
		PBS	18,000	±	0.58
G50sf (1 × 28 cm)	1.5-30	0.1 M Tris-HCl, pH 7.4	9,000	-	0.98
G50sf (1 × 28 cm)		TBS	8,000	-	1.0
G50sf (1 × 47 cm)		TBSE	7,500	-	0.98
G50sf (1 × 47 cm)		50 mM ammonium acetate, pH 7.4	5,000	-	0.98

^a MPD, 2-methyl-2,4-pentanediol; PBS, phosphate-buffered saline; TBS, Tris-buffered saline; TBSE, 0.02 M Tris-HCl, pH 7.4, containing 0.1 M NaCl and 50 μ M EDTA.

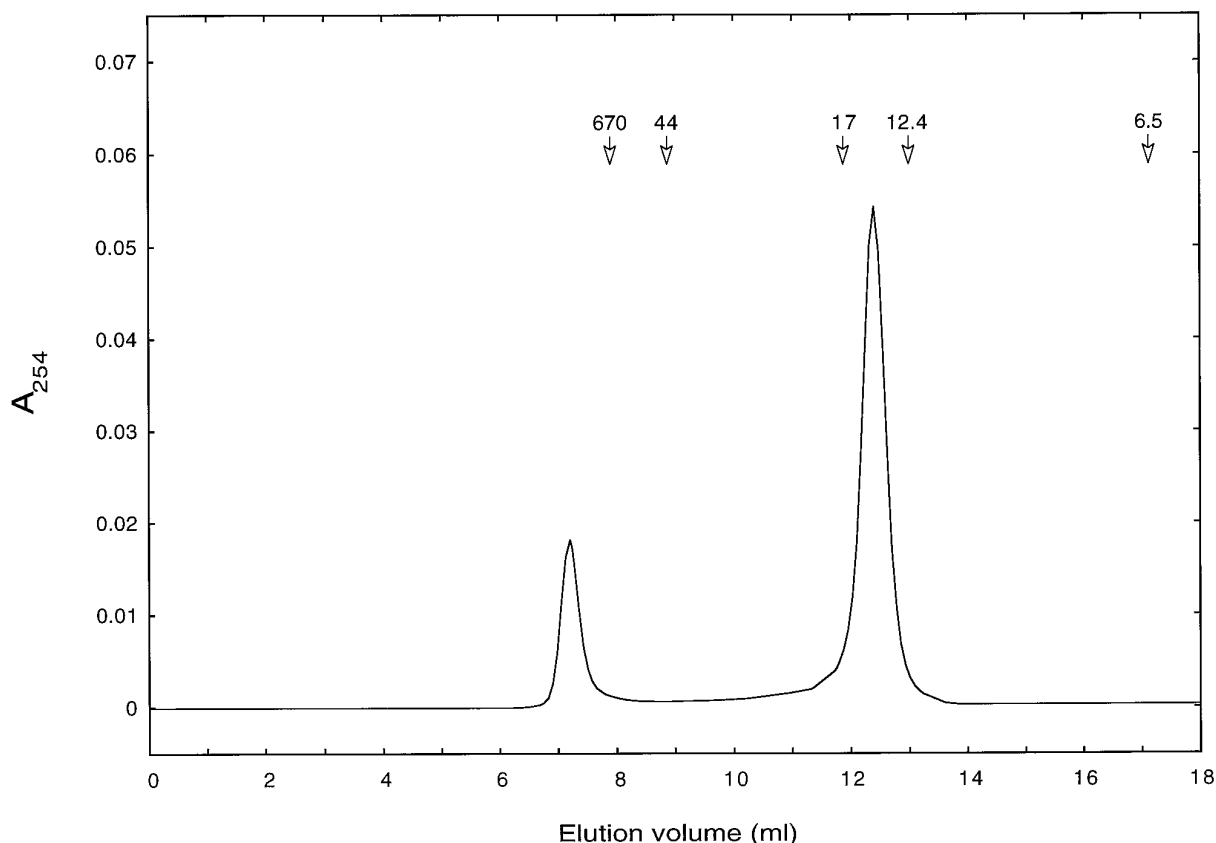


FIG. 1. **Size exclusion chromatography of $A\beta$.** $A\beta$ (1-40) was dissolved in 0.1 M Tris buffer at a concentration of 2 mg/ml and chromatographed on a Superdex 75 column, as described under "Experimental Procedures." The gel-included peak elutes at \sim 12.4 ml, while the gel-excluded peak elutes at \sim 7.2 ml. Elution positions of molecular weight standards are indicated by arrows. Molecular masses are indicated in kDa.

$A\beta$ (1-40) on the Superdex 75/Tris-HCl system (data not shown).

A time-dependent decrease in the magnitude of the gel-included peak was observed under all conditions examined (data not shown). In the Superdex 75/Tris-HCl system, this decrease was accompanied by the appearance of a new peak in

the void volume of the column (Fig. 1). For linear polymers such as dextran, this would be consistent with a molecular weight in excess of 30,000. To better estimate the size of the aggregates in this peak, chromatography was also performed on Superdex 200 and Superose 12 columns, which have exclusion limits (for dextrans) of \sim 100 kDa. A peak was observed in the void volume

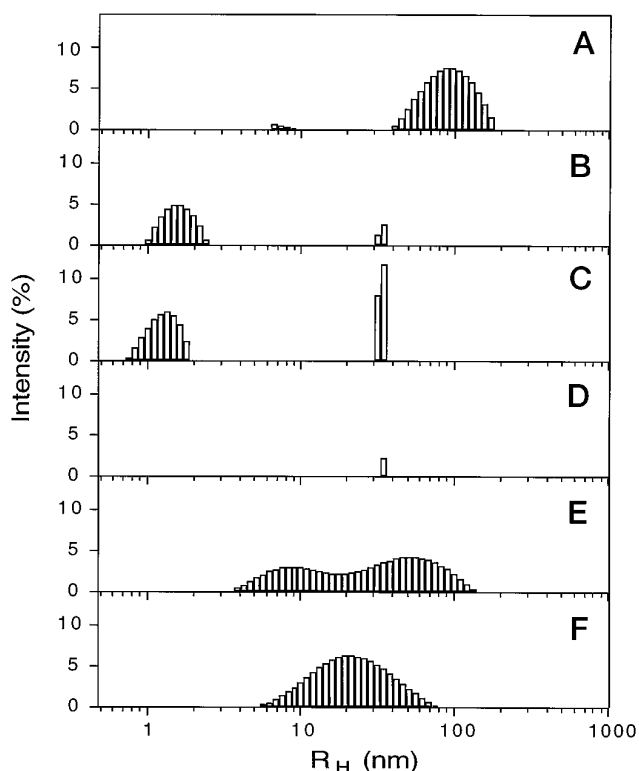


FIG. 2. Analysis of A β size by QLS. Samples included soluble A β (1–40) obtained by dissolution in 0.1 M Tris-HCl and centrifugation for 3 min at $17,000 \times g$ (A); the gel-included fraction obtained following SEC of the supernatant from A (B); aprotinin (6,500 Da) (C); buffer alone (D); soluble A β (1–40) following dissolution in 0.1 M Tris-HCl, incubation at room temperature for 48 h, and centrifugation for 3 min at $17,000 \times g$ (E); and the gel-excluded fraction obtained by SEC of A β (1–40) (F) prepared as in E. Each R_H distribution was normalized to 100% intensity. In A, E, and F, scattering intensity comes predominately from polymeric and aggregated A β . In B, C, and D, scattering from the buffer ($R_H < 0.2$ nm; data not shown) accounts for the remaining scattering, and signals at 35 nm are not peptide-related, since they are present in buffer alone. Comparison of the magnitudes of intensities among experiments is not meaningful.

of these columns as well, suggesting that the A β multimers had molecular masses in excess of 100 kDa, or that they too behaved anomalously on SEC. Experiments using A β (1–42) yielded essentially identical results (data not shown).

Size Determination of A β —To estimate the actual sizes of A β particles in the peaks obtained by SEC, QLS was used to measure the average diffusion coefficient of the particles. Particle size is expressed as the radius of a sphere with an identical diffusion coefficient. This quantity is termed the hydrodynamic radius (R_H) (for a review, see Ref. 28) and is conceptually equivalent to a Stoke's radius in gel permeation chromatography. For spherical particles, $R_H = r$, where r is the geometric radius. For a fibril, R_H depends on the length, diameter, and flexibility of the particle. R_H is always less than the radius of the sphere circumscribed around the particle.

Immediately after dissolution in Tris-HCl and centrifugation ($17,000 \times g$, 3 min), but prior to SEC, soluble A β (1–40) had an average R_H of ~ 40 – 200 nm (Fig. 2A). Because scattering intensity is proportional to molecular weight, monomers and small oligomers can be difficult to detect in the presence of larger polymers and aggregates. However, by fractionating the A β mixture using SEC, we observed a gel-included fraction, with an extrapolated molecular weight of 15,000, which had an average R_H of 1.8 ± 0.2 nm (Fig. 2B). Geometric considerations predict that a 4,331-Da peptide in dimeric form will have a $R_H = 1.5$ – 2.1 nm. For comparison, QLS analysis of aprotinin

(6,500 Da) fractionated by SEC yielded an average R_H of 1.6 ± 0.6 nm (Fig. 2C). These data argue that A β existed as a dimer² in the gel-included fraction, not as a trimer or tetramer as suggested by SEC.

We next sought to determine the size(s) of the A β oligomers in the gel-excluded fraction. To produce sufficient material for analysis, A β (1–40) was incubated for 48 h prior to chromatography. QLS analysis of the pre-SEC supernatant ($17,000 \times g$) revealed a broad distribution of particles sizes (range 4 to >100 nm) (Fig. 2E). Comparison of this distribution with that obtained from A β immediately after dissolution (Fig. 2A) shows that particles of intermediate size form during fibrillogenesis. Dimers were not resolved clearly in this experiment due to the predominance of larger A β oligomers/polymers, as discussed above. QLS analysis of the gel-excluded peak showed that the majority of intermediate particles ranged in size from ~ 10 to 50 nm (Fig. 2F). For a solution of noninteracting rods with diameters of 8 nm, this range corresponds to lengths of 30–500 nm. These lengths would be significantly smaller if rod-rod interactions were occurring. On the other hand, if the rods were flexible, the lengths would be even larger.

Taken together, our SEC and QLS data indicate that the gel-included peak contained dimeric A β , the gel-excluded peak contained a distribution of oligomers, and the pellet obtained prior to chromatography was composed of higher molecular weight polymers and aggregates.

Morphology of A β Oligomers—To determine the morphology of the A β species observed in the SEC experiments, electron microscopy was performed. For both A β (1–40) and A β (1–42), no structures were detected in the gel-included fractions, while the $17,000 \times g$ pellets obtained prior to chromatography contained a mesh of fibers 6–10 nm in diameter (Fig. 3, A and B). These fibers were indistinguishable from those found in senile plaques (29). In addition, particularly in the case of A β (1–42), short fibrils were seen associated with the longer fibers. Generally, one end of each fibril appeared to adhere to the side of a fiber, while the other end was free. Similar fibrils were found in the void volume peaks, where they appeared as short, curly fibrils 6–10 nm in diameter and 5–160 nm in length, on average (Fig. 3, C and D). We have termed these structures “protofibrils” to distinguish them from the mature, amyloid-type fibers found in the pellets.

Chromatographic Analysis of Seedless A β —Low molecular weight oligomers (larger than dimers) were not detected in the prior SEC experiments. Oligomerization could be thermodynamically unfavorable or be suppressed kinetically due to rapid consumption of precursor by growing fibrils. Fibril formation would be accelerated by the presence of pre-existing aggregates (seeds) in the starting material. Freshly prepared solutions of A β (1–40) did, in fact, contain high molecular weight species that might act as seeds (Fig. 2A). To determine if rapid fibril formation affected A β oligomerization, we sought to eliminate seeds prior to our experiments by dissolving A β in HFIP, lyophilizing the solution, dissolving the lyophilizate in Me₂SO, and then filtering the solution through a filter containing 20-nm pores. The chromatographic behavior of peptides “deseeded” in this way did not differ from that of peptides prepared without deseeding (data not shown). An included peak was observed initially, which was replaced over time by a peak in the void volume of the column. These data suggest that formation of stable low molecular weight oligomers is a relatively unfavored process.

High Sensitivity Monitoring of A β Polymerization—Our re-

² For simplicity, A β within the gel-included peak will be referred to as “dimeric.” However, the QLS data alone do not eliminate the possibility that A β within this peak is monomeric.

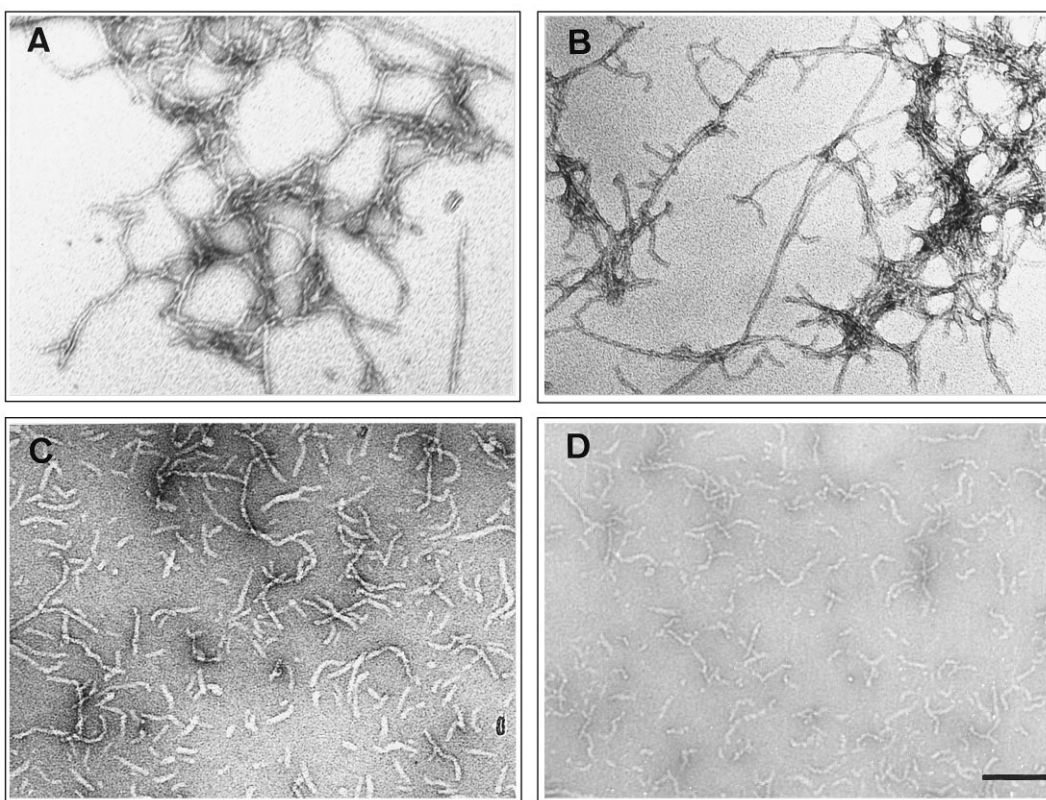


FIG. 3. **Morphology of $A\beta$ polymers fractionated by size exclusion chromatography.** Electron microscopy was performed on prechromatography pellets of $A\beta$ (1-40) (A) and $A\beta$ (1-42) (B) and on the void peaks of $A\beta$ (1-40) (C) and $A\beta$ (1-42) (D). Scale bar, 100 nm.

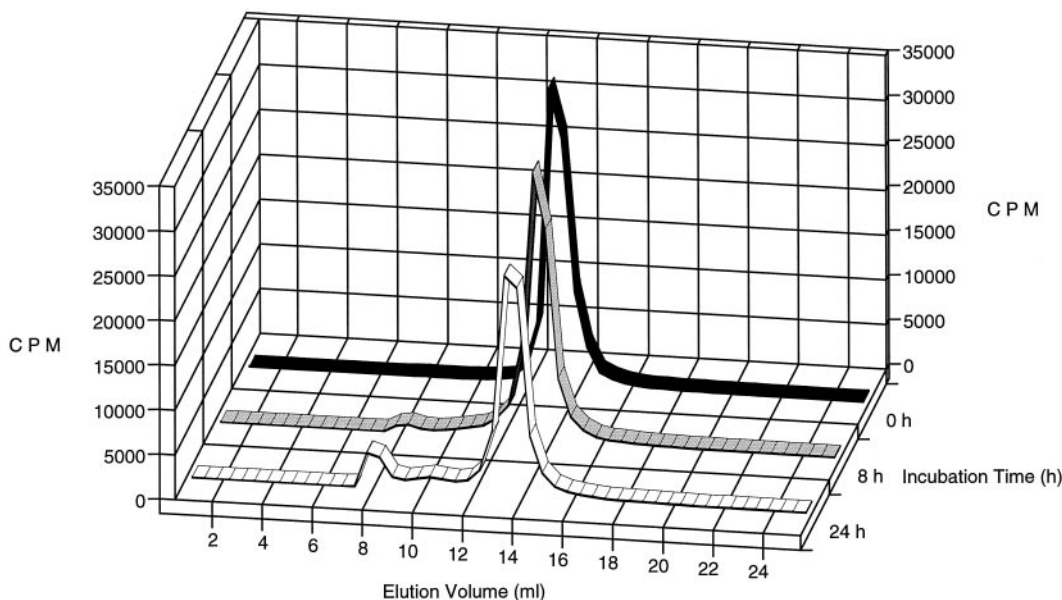


FIG. 4. **High sensitivity size exclusion chromatography of $A\beta$ (1-40).** ^{125}I - $A\beta$ (1-40) was added to a freshly prepared solution of $A\beta$ (1-40) (1 mg/ml) and fractionated on a Superdex 75 column after 0, 8, and 24 h of incubation. The ^{125}I - $A\beta$ (1-40) content of the fractions was determined by scintillation counting. The chromatograms shown are representative of results from three independent experiments.

sults suggested that, if present, steady state levels of oligomeric fibril precursors would be extremely low, making their detection by UV absorbance difficult. For this reason, two sensitive methods were utilized to monitor $A\beta$ polymerization: 1) radioiodinated peptide was used as a tracer in mixtures with unlabeled peptide; and 2) SEC fractions were assayed for $A\beta$ content by RIA. Radioiodinated $A\beta$ (1-40) (^{125}I - $A\beta$ (1-40); 100 pM final concentration) was mixed with unlabeled $A\beta$ (1 mg/ml) in 0.1 M Tris-HCl, pH 7.4, chromatographed on a Superdex 75

column, and detected in column fractions by scintillation counting. At 0 h, a single peak was observed coincident with unlabeled $A\beta$ (Fig. 4). After incubation at room temperature for 8 or 24 h, an additional peak of radioactivity was detected in the void volume (Fig. 4; at ~ 7.4 ml). The radioactivity and UV absorbance of this peak increased at the same rate over time, suggesting that the labeled and unlabeled peptides polymerized in an analogous manner.

In the above experiment, given that $\sim 33,000$ cpm of $A\beta$ were

used, oligomers representing as little as 1% of the initial protein mass could have been detected. Asymmetry in the void and dimer peaks, indicated by trailing and leading shoulders, respectively, mirrored the behavior of the unlabeled peptide (*cf.* Figs. 1 and 4). RIA analysis of $A\beta$ -(1–40) SEC fractions produced using the same protocol as above yielded results similar to those presented in Fig. 4 (data not shown). Experiments were also performed at much lower $A\beta$ concentrations by using tracer alone; however, below 10^{-5} M, recovery of ^{125}I - $A\beta$ -(1–40) from the column was poor, probably due to nonspecific adsorption to the column matrix and associated glass and plastic surfaces (22, 30). Taken together, these data suggest that although oligomeric intermediates do exist, they do not accumulate to a significant degree during the polymerization process.

Kinetics of Protofibril Formation—As a first step to determining the key primary structural elements of $A\beta$ that control the kinetics of dimer and protofibril utilization, comparative polymerization studies were done using $A\beta$ -(1–42), $A\beta$ -(1–40), and $A\beta$ -(1–40) containing the substitutions Phe¹⁹ \rightarrow Pro (31), Ala²¹ \rightarrow Gly (32), or Glu²² \rightarrow Gln (33). Peptides were dissolved in Tris-HCl, pH 7.4, at concentrations of 1 mg/ml, incubated for up to 24 h, and then their polymerization states were analyzed by SEC on a Superdex 75 column.

Immediately after dissolution, all samples produced a single chromatographic peak with a retention time equivalent to that of dimeric wild type $A\beta$ -(1–40). The level of the $A\beta$ -(1–40) peak declined by $\sim 20\%$ over 24 h, while the levels of the $A\beta$ -(1–40)-Pro¹⁹ and $A\beta$ -(1–40)-Gly²¹ peaks declined $<10\%$ (Fig. 5A). $A\beta$ -(1–42) and $A\beta$ -(1–40)-Gln²² peaks decreased rapidly initially, with a $\sim 40\%$ decrease within 1 h, followed by a slower decrease down to 20–30% of initial levels by 24 h (Fig. 5A). The inverse was observed for the protofibril peaks (Fig. 5B). The levels of protofibrils produced by $A\beta$ -(1–40) and $A\beta$ -(1–40)-Gly²¹ increased ~ 15 and $\sim 5\%$, respectively, over the first 24 h. No protofibril peak was detected at 24 h in experiments with $A\beta$ -(1–40)-Pro¹⁹. In contrast, the levels of protofibrils formed by $A\beta$ -(1–42) and $A\beta$ -(1–40)-Gln²² increased rapidly within the first hour. Peak levels of protofibrils were seen after 8 h for $A\beta$ -(1–42) and after 1 h for $A\beta$ -(1–40)-Gln²², after which these levels declined. The continuous decline in levels of the included peak, coupled with the transitory appearance of protofibrils, is consistent with the protofibril being an intermediate in $A\beta$ fibrillogenesis.

SDS-PAGE of $A\beta$ Oligomers—SDS-stable oligomers have been detected previously in media from cultured cells secreting $A\beta$ (34). To determine the SDS stability of the oligomers observed during SEC, peak fractions were analyzed by SDS-PAGE. Interestingly, dimer, protofibril (void), and fiber (pellet) fractions produced during polymerization of $A\beta$ -(1–40) all produced a single 4-kDa band (Fig. 6A). To identify trace levels of oligomers, ^{125}I - $A\beta$ -(1–40) was incubated with $A\beta$ -(1–40), and the resulting products were characterized autoradiographically following gel electrophoresis. A single 4-kDa band was observed in this experiment as well (data not shown). Electrophoresis of SEC fractions of $A\beta$ -(1–42) produced a different pattern (Fig. 6B). Void peak fractions produced five bands, corresponding in mass to monomeric through pentameric $A\beta$ (Fig. 6B, lanes 2–4). The dimer peak of $A\beta$ -(1–42) ran as a single 4.5-kDa band (Fig. 6B, lanes 5 and 6). Prechromatography pellets (see “Experimental Procedures”), which contained fully formed $A\beta$ fibers, produced the same five bands as did the void peak fractions, plus an occasional gel-excluded band (Fig. 6B, lane 1). These data show that SDS disaggregates $A\beta$ fibers and protofibrils down to monomers, in the case of $A\beta$ -(1–40), or to monomers and low molecular weight oligomers, in the case of $A\beta$ -(1–42).

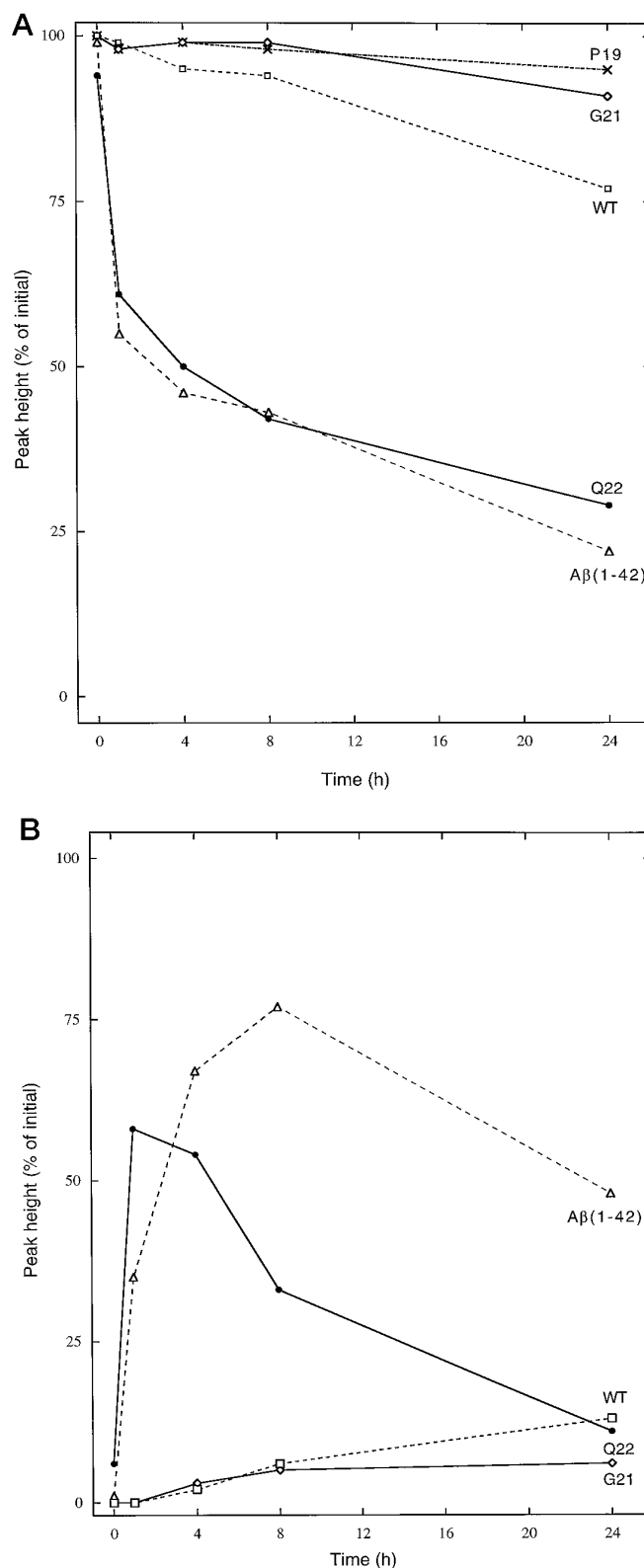


FIG. 5. Kinetics of $A\beta$ polymerization. $A\beta$ peptides were allowed to polymerize for 0, 1, 4, 8, and 24 h and then were fractionated by SEC (see “Experimental Procedures”). Amounts of dimeric $A\beta$ (A) and protofibrils (B) are plotted as a percentage of the levels at time 0, which were assigned a value of 100%. Experiments were done in duplicate. WT, wild type; P19, Phe¹⁹ \rightarrow Pro; G21, Ala²¹ \rightarrow Gly; Q22, Glu²² \rightarrow Gln.

DISCUSSION

Accumulating evidence supports the hypothesis that $A\beta$ fibrillogenesis is a seminal pathogenetic event in AD (35, 36).

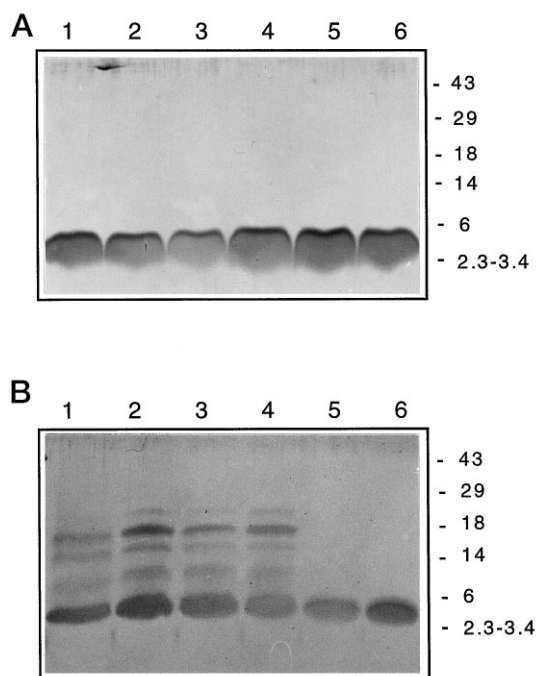


FIG. 6. SDS-PAGE analysis of SEC fractions. $A\beta$ -(1-40) (A) and $A\beta$ -(1-42) (B) were dissolved in 0.1 M Tris-HCl, pH 7.4, incubated 6–48 h, and then analyzed by SEC, as described under “Experimental Procedures.” The prechromatography pellets (lanes 1), void peak fractions (lanes 2–4), and fractions from the dimer peaks (lanes 5–6) were then analyzed by SDS-PAGE and silver staining.

Inhibiting or reversing fibrillogenesis is thus a logical therapeutic strategy. The goal of the experiments reported here was to characterize, structurally and kinetically, the initial stages of $A\beta$ fibrillogenesis to identify targets for fibrillogenesis inhibitors. We have discovered a potential target, the amyloid protofibril, which appears to be an important intermediate in $A\beta$ fibrillogenesis. This discovery, and the unique constellation of methods used to achieve it, have implications both for our understanding of $A\beta$ fibrillogenesis and for the methodological approaches used to study $A\beta$ polymerization.

In our SEC studies of $A\beta$ -(1-40) polymerization, a single peak was observed following dissolution of lyophilized peptide (Table I). The M_r of this peak varied from 5 to 18 kDa, depending on the solvents and columns used, corresponding to monomeric to tetrameric $A\beta$. These molecular weight estimations and, in fact, those of other groups using SEC (20–23, 37, 38) were based on calibration curves derived using soluble peptides and proteins specially selected for their ideal chromatographic behavior. However, we found that $A\beta$, under nondenaturing conditions, did not chromatograph ideally. This behavior is not uncommon for amphipathic peptides, such as $A\beta$, which may undergo both electrostatic and/or hydrophobic interactions with the column matrix (39). For example, nonideal chromatographic behavior has recently been reported for both the nonamyloid component of AD amyloid (40) and melittin (41). Therefore, to be able to estimate accurately the molecular weights, and thus the oligomerization states, of $A\beta$ using SEC, new standardization methods had to be utilized.

QLS is a particularly powerful and appropriate technique for monitoring the sizes of protein polymers in solution (for a review, see Ref. 28). By coupling SEC with QLS, the oligomerization state of $A\beta$ within different chromatographic fractions could be estimated directly, rapidly, and noninvasively. We found that $A\beta$ -(1-40) and $A\beta$ -(1-42) exhibit predominantly three forms in aqueous solution: dimer, protofibril, and fiber. Metastable oligomers (dimer $< M_r <$ protofibril) were detected

using highly sensitive radiochemical and immunological assays; however, none accumulated in significant quantities. $A\beta$ -(1-40) and $A\beta$ -(1-42) have been reported to form stable dimers (20, 23) as well as high molecular weight polymers (20), although these latter structures were not characterized. Our analysis of protofibril fractions by QLS revealed a R_H distribution of 10–50 nm. Assuming $A\beta$ forms rods with an 8-nm average diameter, and recognizing that in polydisperse populations of polymers the larger particles skew the R_H distribution toward higher values, the QLS data were consistent with protofibrils 30–500 nm in length. These estimates were consistent with results of electron microscopy, which revealed curly fibrils 6–10 nm in diameter and ranging in length up to 200 nm.

An important question arising from the discovery of the protofibril was where it lay in the pathway of $A\beta$ fibrillogenesis. In an effort to answer this question, SEC was used to study the stages and kinetics of $A\beta$ fibrillogenesis. In the cases of $A\beta$ -(1-42) and $A\beta$ -(1-40)-Gln²², dimers predominated initially, and then a time-dependent decrease in dimer levels was paralleled by an increase in protofibrils. Finally, protofibril levels declined as well. Radiochemical analyses of SEC fractions showed that only two discrete $A\beta$ species, dimer and protofibril, accumulated during fibrillogenesis. However, trailing and leading shoulders associated with protofibril and dimer peaks, respectively, appeared during fibrillogenesis. In addition, an elevated base line was observed between the protofibril and dimer peaks. These data are consistent with a polymerization process in which $A\beta$ oligomerizes through a series of short lived intermediates to form protofibrils, which act as centers for the growth of mature fibers. A similar pathway has been proposed by Harper *et al.* (42) based on studies of $A\beta$ polymerization monitored by atomic force microscopy.

Rates of dimer utilization and protofibril formation varied markedly among different $A\beta$ species (Fig. 5). The differences observed agree qualitatively with previous reports indicating that structural elements in the central hydrophobic core (Leu¹⁷-Ala²¹) and at the COOH terminus of $A\beta$ play key roles in controlling fibrillogenesis (7, 11, 43–46). For example, relative to wild type $A\beta$ -(1-40), both $A\beta$ -(1-40)-Gln²² and $A\beta$ -(1-42) polymerize into protofibrils and then into fibers significantly faster. In each case, amino acid substitutions (Glu²² \rightarrow Gln²²) or additions (Ile⁴¹-Ala⁴²) produce peptides of greater hydrophobicity, a change that could drive aggregation through the hydrophobic effect (47). Whether significant intramolecular or intermolecular structural changes also contribute to the altered kinetics is unknown. In contrast, $A\beta$ -(1-40)-Gly²¹ polymerized more slowly than did wild type peptide, while $A\beta$ -(1-40)-Pro¹⁹ remained almost completely unpolymerized. Few protofibrils were formed by $A\beta$ -(1-40)-Gly²¹ after 24 h, and none were observed in the $A\beta$ -(1-40)-Pro¹⁹ samples. These results suggest that glycine and proline alter $A\beta$ structure in a manner that inhibits or precludes the self-associations necessary to produce protofibrils and fibers. This could occur through destabilization of structural elements, including α -helices and/or β -strands (48, 49), required for fiber formation. This mechanism has been implicated in alterations in β PP processing induced by familial AD mutations (31, 50) and is consistent with previous findings that fibril formation requires formation of a stable β -sheet structure (11, 44, 51, 52).

In addition to SEC, denaturing gel electrophoresis (SDS-PAGE) has been used to characterize $A\beta$ oligomers (17–20). However, on theoretical grounds (*i.e.* the use of the chaotrope SDS), this technique would be expected to disaggregate noncovalent complexes, limiting its usefulness in studies of protein aggregation. We examined this issue by comparing results

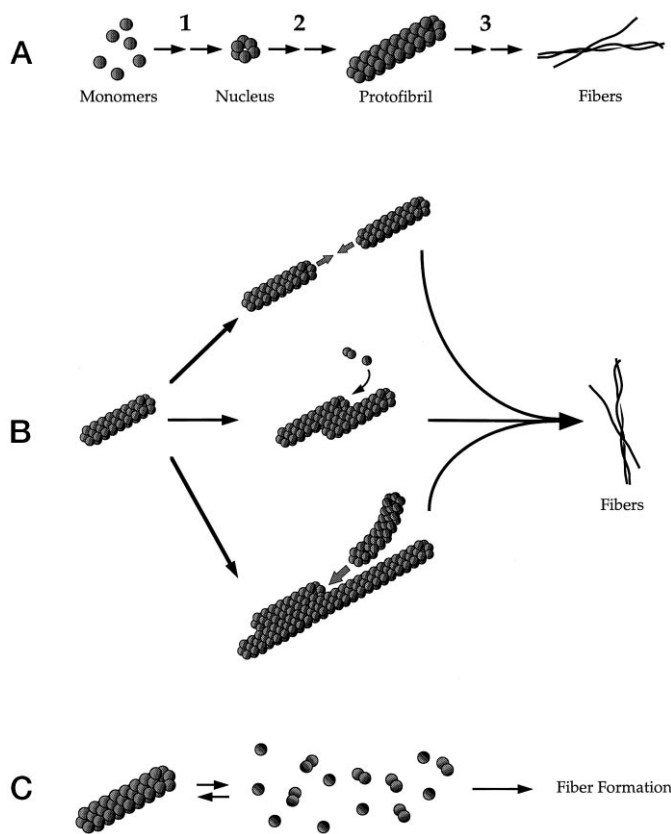


FIG. 7. **Models of A β fibrillogenesis.** *A*, A β fibrillogenesis is a nucleation-dependent polymerization process in which monomeric A β forms nuclei (step 1) from which protofibrils emanate (step 2). These protofibrils give rise to full-length fibers (step 3). *B*, dimers may form nuclei and add to them or to protofibrils, directly. However, dimers may also be in equilibrium with monomers, which might themselves act as the building blocks for these polymeric structures. *C*, besides the addition of A β to protofibril ends, protofibrils may give rise to mature fibers through simple end-to-end annealing; lateral association of protofibrils, followed by A β addition to ends; and lateral association followed by end-to-end annealing. *D*, it is also possible that protofibrils are incapable of forming fibers directly but instead simply provide precursors for productive pathways of fibrillogenesis. Note that A β and its oligomers are not drawn to scale.

obtained by SEC/QLS with those from SDS-PAGE. Fibers, protofibrils, and dimers of A β (1–40) all produced a single ~4-kDa band on gels (Fig. 6A). A single band was also seen with dimeric A β (1–42), whereas A β (1–42) protofibrils and fibers produced essentially identical ladders of low molecular weight species ranging from monomer to pentamer (Fig. 6B). These results show clearly that SDS-PAGE data do not reliably reflect the polymerization state of A β under native conditions. However, the technique may be of use in the characterization of factors that produce detergent-stable multimers.

Modeling A β Fibrillogenesis—The structural and kinetic analyses of A β fibrillogenesis presented here revealed the existence of a previously unidentified fiber intermediate, the protofibril. The data extant are consistent with a number of models of protofibril formation and conversion into fibers. Each model posits that A β monomers combine to form fibril nuclei (Fig. 7A, step 1), from which protofibrils emanate by linear growth (Fig. 7A, step 2). These protofibrils, in turn, give rise to the classical 6–10-nm fibers characteristic of neuritic plaques (Fig. 7A, step 3). During fibrillogenesis, A β dimers accumulate initially and then are consumed as protofibrils and fibers form. These dimers may be involved directly in steps 1–3 or may be in equilibrium with monomers, which could be the true building blocks for nuclei, protofibrils, and/or fibers. A dimer “res-

ervoir” could control the monomer concentration and, therefore, the kinetics of fibrillogenesis in the way micelles control fibrillogenesis kinetics at low pH (8, 53).

A number of mechanisms may explain the protofibril→fiber transition (Fig. 7B). The simplest is end-to-end association of protofibrils. This is unlikely, however, because of the kinetic barriers associated with the diffusion and proper alignment of protofibril ends. Protofibrils could associate laterally to form “self-templates,” onto which precursors (dimers/monomers) could bind and polymerize. Alternatively, lateral association of protofibrils could accelerate end-to-end annealing by fostering proper alignment of protofibril ends. It is also possible that protofibrils are the end-products of a nonfibrillogenic pathway (Fig. 7C). In this case, protofibril dissociation would be necessary to release A β precursors into productive pathways of fiber formation. Experiments are currently under way to discriminate among these possibilities. Initial results suggest that protofibrils self-associate to produce fibers in the absence of low molecular weight precursors.³ This mechanism is supported by the failure to observe a continuous distribution of fiber lengths in the size domain between protofibrils and mature amyloid fibers (42).³

If protofibrils are key intermediates in A β fibrillogenesis *in vivo*, as they appear to be *in vitro*, they would be attractive therapeutic targets because 1) fibrillogenesis mediated through protofibrils might be poisoned with as little as one or two inhibitor molecules per protofibril, and 2) fibrillogenesis inhibitors would function extracellularly. In particular, because the therapeutic levels of inhibitor in the plasma or cerebrospinal fluid would be orders of magnitude lower than those necessary for inhibitors binding to monomeric A β , the risk of cytotoxic side-effects would significantly decrease.

Acknowledgments—We thank Dr. John Maggio and William Esler for help with the A β RIA, and Marika Ericsson for advice and assistance with electron microscopy. We thank Dr. Peter Lansbury for discussing unpublished data.

REFERENCES

- Selkoe, D. J. (1991) *Neuron* **6**, 487–498
- Glenner, G. G., and Wong, C. W. (1984) *Biochem. Biophys. Res. Commun.* **120**, 885–890
- Seubert, P., Vigo-Pelfrey, C., Esch, F., Lee, M., Dovey, H., Davis, D., Sinha, S., Schlossmacher, M. G., Whaley, J., Swindlehurst, C., McCormack, R., Wolfert, R., Selkoe, D. J., Lieberburg, I., and Schenk, D. (1992) *Nature* **359**, 325–327
- Busciglio, J., Gabuzda, D. H., Matsudaira, P., and Yankner, B. A. (1993) *Proc. Natl. Acad. Sci. U. S. A.* **90**, 2092–2096
- Selkoe, D. J. (1994) *J. Neuropathol. Exp. Neurol.* **53**, 438–447
- Yankner, B. A. (1996) *Nat. Med.* **2**, 850–852
- Jarrett, J. T., and Lansbury, P. T., Jr. (1993) *Cell* **73**, 1055–1058
- Lomakin, A., Chung, D. S., Benedek, G. B., Kirschner, D. A., and Teplow, D. B. (1996) *Proc. Natl. Acad. Sci. U. S. A.* **93**, 1125–1129
- LeVine, H., III (1993) *Protein Sci.* **2**, 404–410
- Clements, A., Walsh, D. M., Williams, C. H., and Allsop, D. (1993) *Neurosci. Lett.* **161**, 17–20
- Clements, A., Allsop, D., Walsh, D. M., and Williams, C. H. (1996) *J. Neurochem.* **66**, 740–747
- Mantyh, P. W., Ghilardi, J. R., Rogers, S., DeMaster, E., Allen, C. J., Stimson, E. R., and Maggio, J. E. (1993) *J. Neurochem.* **61**, 1171–1174
- Snyder, S. W., Lador, U. S., Wade, W. S., Wang, G. T., Barrett, L. W., Matayoshi, E. D., Huffaker, H. J., Krafft, G. A., and Holzman, T. F. (1994) *Biophys. J.* **67**, 1216–1228
- Cohen, R. J., and Benedek, G. B. (1975) *Immunochemistry* **12**, 349–351
- Tomski, S. J., and Murphy, R. M. (1992) *Arch. Biochem. Biophys.* **294**, 630–638
- Shen, C.-L., Scott, G. L., Merchant, F., and Murphy, R. M. (1993) *Biophys. J.* **65**, 2383–2395
- Hilbich, C., Kisters-Woike, B., Reed, J., Masters, C., and Beyreuther, K. (1991) *J. Mol. Biol.* **218**, 149–163
- Burdick, D., Soreghan, B., Kwon, M., Kosmoski, J., Knauer, M., Henschen, A., Yates, J., Cotman, C., and Glabe, C. (1992) *J. Biol. Chem.* **267**, 546–554
- Pike, C. J., Burdick, D., Walencewicz, A. J., Glabe, C. G., and Cotman, C. W. (1993) *J. Neurosci.* **13**, 1676–1687
- Soreghan, B., Kosmoski, J., and Glabe, C. (1994) *J. Biol. Chem.* **269**, 28551–28554

³ D. M. Walsh and D. B. Teplow, unpublished observations.

21. Barrow, C. J., Yasuda, A., Kenny, P. T. M., and Zagorski, M. (1992) *J. Mol. Biol.* **225**, 1075–1093
22. Bush, A. I., Pettingell, W. H., Jr., de Paradis, M., and Tanzi, R. E. (1994) *J. Biol. Chem.* **269**, 12152–12158
23. Kametani, F., Tanaka, K., Tokuda, T., and Allsop, D. (1995) *Brain Res.* **703**, 237–241
24. Naslund, J., Karlstrom, A. R., Tjernberg, L. O., Schierhorn, A., Terenius, L., and Nordstedt, C. (1996) *J. Neurochem.* **67**, 294–301
25. Maggio, J. E., Stimson, E. R., Ghilardi, J. R., Allen, C. J., Dahl, C. E., Whitcomb, D. C., Vigna, S. R., Vinters, H. V., Labenski, M. E., and Mantyh, P. W. (1992) *Proc. Natl. Acad. Sci. U. S. A.* **89**, 5462–5466
26. Esler, W. P., Stimson, E. R., Jennings, J. M., Ghilardi, J. R., Mantyh, P. W., and Maggio, J. E. (1996) *J. Neurochem.* **66**, 723–732
27. Schagger, H., and Von Jagow, G. (1987) *Anal. Biochem.* **166**, 368–379
28. Pecora, R. (1985) *Dynamic Light Scattering: Applications of Photon Correlation Spectroscopy* (Pecora, R., ed), Plenum Press, New York, NY
29. Kirschner, D. A., Abraham, C., and Selkoe, D. J. (1986) *Proc. Natl. Acad. Sci. U. S. A.* **83**, 503–507
30. Chan, W., Fornwald, J., Brawner, M., and Wetzel, R. (1996) *Biochem.* **35**, 7123–7130
31. Haass, C., Hung, A. Y., Selkoe, D. J., and Teplow, D. B. (1994) *J. Biol. Chem.* **269**, 17741–17748
32. Hendriks, L., Van Duijn, C. M., Cras, P., Cruts, M., Van Hul, W., Van Harskamp, F., Warren, A., McInnis, M. G., Antonarakis, S. E., Martin, J.-J., Hofman, A., and Van Broeckhoven, C. (1992) *Nat. Genet.* **1**, 218–221
33. Levy, E., Carman, M. D., Fernandez-Madrid, I. J., Power, M. D., Lieberburg, I., van Duinen, S. G., Bots, G. T. A. M., Luyendijk, W., and Frangione, B. (1990) *Science* **248**, 1124–1126
34. Podlisny, M. B., Ostaszewski, B. L., Squazzo, S. L., Koo, E. H., Rydell, R. E., Teplow, D. B., and Selkoe, D. J. (1995) *J. Biol. Chem.* **270**, 9564–9570
35. Haass, C. (1996) *Eur. Arch. Psych. Clin. Neurosci.* **246**, 118–123
36. Selkoe, D. J. (1996) *J. Biol. Chem.* **271**, 18295–18298
37. Roher, A. E., Chaney, M. O., Kuo, Y. M., Webster, S. D., Stine, W. B., Haverkamp, L. J., Woods, A. S., Cotter, R. J., Tuohy, J. M., Krafft, G. A., Bonnell, B. S., and Emmerling, M. R. (1996) *J. Biol. Chem.* **271**, 20631–20635
38. Roher, A., Wolfe, D., Palutke, M., and KuKuruga, D. (1986) *Proc. Natl. Acad. Sci. U. S. A.* **83**, 2662–2666
39. Irvine, G. B. (1997) *Anal. Chem. Acta.*, in press
40. Weinreb, P. H., Zhen, W. G., Poon, A. W., Conway, K. A., and Lansbury, P. T., Jr. (1996) *Biochem.* **35**, 13709–13715
41. Perez-Paya, E., Houghten, R. A., and Blondelle, S. E. (1995) *J. Biol. Chem.* **270**, 1048–1056
42. Harper, J. D., Wong, S. S., Lieber, C. M., and Lansbury, P. T., Jr. (1997) *Chem. Biol.* **4**, 119–125
43. Jarrett, J. T., Berger, E. P., and Lansbury, P. T., Jr. (1993) *Biochemistry* **32**, 4693–4697
44. Soto, C., and Castano, E. M. (1996) *Biochem. J.* **314**, 701–707
45. Soto, C., Castano, E. M., Frangione, B., and Inestrosa, N. C. (1995) *J. Biol. Chem.* **270**, 3063–3067
46. Teplow, D. B., Lomakin, A., Benedek, G. B., Kirschner, D. A., and Walsh, D. M. (1997) in *Alzheimer's Disease: Biology, Diagnosis and Therapeutics* (Iqbal, K., Winblad, B., Nishimura, T., Takeda, M., and Wisniewski, H. M., eds) pp. 311–319, John Wiley & Sons Ltd., Chichester, United Kingdom
47. Dill, K. A. (1990) *Biochemistry* **31**, 7133–7155
48. Richardson, J. S., and Richardson, D. C. (1989) in *Prediction of Protein Structures and the Principles of Protein Conformation* (Fasman, G. D., ed) pp. 1–98, Plenum Publishing Corp., New York
49. Minor, D. L., Jr., and Kim, P. S. (1994) *Nature* **367**, 660–663
50. Sisodia, S. S. (1992) *Proc. Natl. Acad. Sci. U. S. A.* **89**, 6075–6079
51. Soto, C., Castano, E. M., Kumar, R. A., Beavis, R. C., and Frangione, B. (1995) *Neurosci. Lett.* **200**, 105–108
52. Fraser, P. E., McLachlan, D. R., Surewicz, W. K., Mizzen, C. A., Snow, A. D., Nguyen, J. T., and Kirschner, D. A. (1994) *J. Mol. Biol.* **244**, 64–73
53. Lomakin, A., Teplow, D. B., Kirschner, D. A., and Benedek, G. B. (1997) *Proc. Natl. Acad. Sci. U. S. A.* **94**, 7942–7947